An excitation-energy-dependent molecular beacon detects early-stage neurotoxic Aβ aggregates in the presence of cortical neurons.

Christina E. Gulácsy[1], Richard Meade[1], Dragana A.M. Catici[1], Christian Soeller[4], G.Dan Panto[§3], D. Dafydd Jones[5], Dominic Alibhai[6], Mark Jepson[6], Ventsislav K. Valev[2], Jody M. Mason[1]*, Robert J. Williams[1]*, Christopher R. Pudney[1]*

[1]Department of Biology and Biochemistry, [2]Department of Physics, [3]Department of Chemistry, University of Bath, Bath, United Kingdom.[4]Biomedical Physics, University of Exeter, Exeter, United Kingdom.[5]School of Biosciences, Cardiff University, Cardiff, United Kingdom. [6]Wolfson Bioimaging Facility, University of Bristol, Bristol United Kingdom.

KEYWORDS Fluorescence, edge-shift, amyloid beta, Alzheimer's, neuron

ABSTRACT: There is now crucial medical importance placed on understanding the role of early-stage, sub-visible protein aggregation, particularly in neurodegenerative disease. While there are strategies for detecting such aggregates in vitro, there is no approach at present that can detect these toxic species associated with cells and specific subcellular compartments. We have exploited excitation-energy-dependent fluorescence edge-shift of recombinant protein labelled with a molecular beacon, to provide a sensitive read out for the presence of sub-visible protein aggregates. To demonstrate the potential utility of the approach we examine the major peptide associated with the initiation of Alzheimer's disease, amyloid β-protein (Aβ) at a patho-physiologically relevant concentration in mouse cortical neurons. Using our approach, we find preliminary evidence that sub-visible Aβ aggregates are detected at specific subcellular regions and that neurons drive the formation of specific Aβ aggregate conformations. These findings therefore demonstrate the potential of a novel fluorescence-based approach for detecting and imaging protein aggregates in a cellular context, which can be used to sensitively probe the association of early-stage toxic protein aggregates within subcellular compartments.

Neurodegenerative disorders, such as Alzheimer's disease (AD), are major pathological issues facing aging populations across the world. These diseases typically arise coincident with the appearance and deposition of hallmark protein aggregates, many of which are thought to be toxic to neurons.[1] Amyloid β-protein (Aβ) is the major peptide component of senile plaques found in AD, and the present consensus view is that early stage, sub-visible (<1 μm) aggregates composed of small oligomers of Aβ are the likely toxic species.[2,3] Formation of these early-stage aggregates are thought to promote further aggregation, leading to fibrillation of the protein.[1] Early-stage Aβ aggregates can be tracked in isolation for example using FRET based-assays[4] and late-stage fibrillar aggregates can be monitored in cell-based or tissue assays.[5] A range of approaches have been developed for the purpose of capturing increasingly small and early stage protein aggregates, for example emerging super resolution,[6] FRET-based sensor[7] and single molecule approaches.[8,9]

However, there is presently no strategy for monitoring and quantifying the extent of pre-fibrillar, soluble Aβ aggregates associated with cells and in different sub-cellular compartments. Being able to visualize these early stage toxic species within their cellular context would dramatically enhance our ability to understand the molecular mechanisms underlying the development and progression of AD.

Excitation-energy-dependent changes in fluorophore emission are most commonly reported as the red-edge excitation shift (REES).[10-13] That is, the fluorescence emission spectrum of a fluorophore shows a shift in the peak maximum and inhomogeneous broadening of the spectra upon decreasing excitation energy.[11,12] This shift is observed in situations where, after photo-excitation, the solvent relaxation is slow relative to the emission of the fluorophore. This leads to emission from a lower level excited state, shifting the emission to lower energies. When decreasing the excitation energy, discrete emission states are photoselected, resulting in a red-shift of the emission spectrum with respect to excitation wavelength.[10-14] The REES phenomenon has been observed in biomolecules both with intrinsic and extrinsic fluorophores.[14-19] Less commonly observed is a blue-shift in the emission spectrum with decreasing excitation energy, however, this may be explained by upward orientational relaxation of the environment.[20] These concepts are shown in Figure 1A. Experimentally, one measures the combined excitation/emission (EEM) spectrum and plots the change in the center of spectral mass (CSM) of the emission spectra, versus the change in excitation wavelength ($\Delta\lambda_{Ex}$).

Edge-shift phenomena have been shown to be accurate probes of subtle protein conformational change (for example refs 14-18), and we have recently shown sensitivity to changes in the proteins free energy landscape.[15] Given

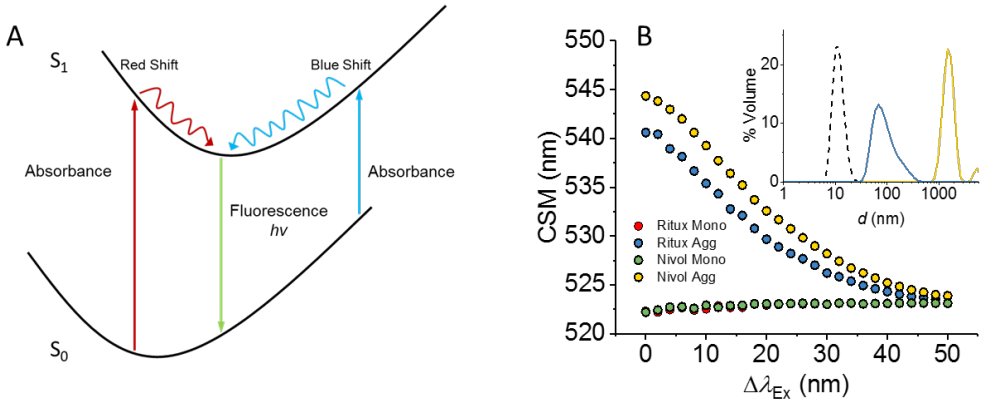

Figure 1. A, Ground and excited electronic states demonstrated by the orientational coordinates of their zero vibrational levels. Relaxation along the potential curve to the energy minimum leads to photo-selected emission causing a red-shift, or blue-shift for up-relaxation. B, Edge-shift measurements of monomeric (red and green) and aggregated (blue and yellow) Rituximab and Nivolumab labelled with Alexa-488. Inset, DLS profiles for monomeric (black dashed line) and aggregated mAbs (colors as main panel).

this sensitivity, we reasoned that early-stage, amorphous protein aggregates would similarly reflect highly complex fluorophore environments. As such, an extrinsic fluorophore label, acting as a molecular beacon, might prove sensitive to aggregate formation when measuring edge-shift. Such a probe would then allow the formation of early stage aggregates to be imaged.

Herein, we demonstrate that the fluorescence edge-shift phenomenon can be used to monitor the formation of early stage, sub-visible Aβ aggregates (< ~1 μm). We detect these species in cultured neurons exposed to nanomolar concentrations of a model peptide fragment[21] responsible for Aβ aggregation (Aβ15-21) as well as near full length peptide (Aβ1-40) and imaged using high resolution microscopy. We find evidence that sub-visible Aβ aggregates associate with discrete subcellular compartments of the neuron, likely due to the presence of specific Aβ binding sites or the influence of the local cellular environment on the formation of a particular Aβ species. Moreover, our data point to the importance of considering Aβ aggregation in the presence of a relevant cellular model and that potentially neurons themselves drive the Aβ aggregation type. Our findings present a new approach for monitoring the formation and interaction of toxic Aβ species with a relevant cellular model system, but also point to a new tool that could be used much more widely to augment basic research and drug development into other neurodegenerative diseases that are driven by protein aggregation.

RESULTS AND DISCUSSION

Antibodies are particularly prone to aggregation and can easily be driven to early stage aggregates through low temperature incubation. Therefore, we wished to use these species as model systems to explore whether protein aggregation could be detected sensitively by extrinsic fluorophore edge-shift. We have labelled two therapeutic monoclonal antibodies (mAbs), Rituximab and Nivolumab, with either the fluorophores Alexa 488 or fluorescein via a maleimide linkage to solvent exposed cysteine residues (Figure S1).

Absorption spectra (Figure S1A-C) show that essentially 0.5 molar equivalents of either dye binds to the mAbs under the conditions we use. Figures S1D-I show the emission spectra for each dye-labelled mAb in both monomeric (Figure S1G-I) and aggregated states (Figure S1G-I). The resulting edge-shift data are shown in Figure 1B for the Alexa488 mAbs and in Figure S2 for the fluorescein labelled mAb. Figure 1B inset, shows dynamic light scattering (DLS) data for the mAbs, providing independent evidence that the thermally treated mAbs have formed sub-visible aggregates. From Figure 1B we find that the native, non-aggregated protein displays no edge-shift across the excitation range studied. However, we find on thermal aggregation of the mAbs, for both Alexa 488 and fluorescein, there is a clear blue-shift in the emission spectra (Figure 1B and S2). Moreover, the trend is the same with two different fluorophores, demonstrating our observation is not an artefact of a specific dye structure. The excitation spectra are essentially invariant across the emission range studied, for both the monomeric and aggregated mAbs as shown in Figure S1J-L, demonstrating that the observed edge-shift does not have an artefactual cause.

The monomeric mAb labelled with fluorescein shows some blue-shift in its emission spectra (Figure S2). However, the overall magnitude is far smaller than that observed for the aggregated protein. From Figure 1B, the data show that the magnitude of the blue-shift plateaus as the aggregates tend towards visible particles (>1 μm). Based on the observed changes the observed edge shift appear to saturate towards aggregates in the ~100mer region. Therefore, these data suggest that the blue-shift is primarily sensitive

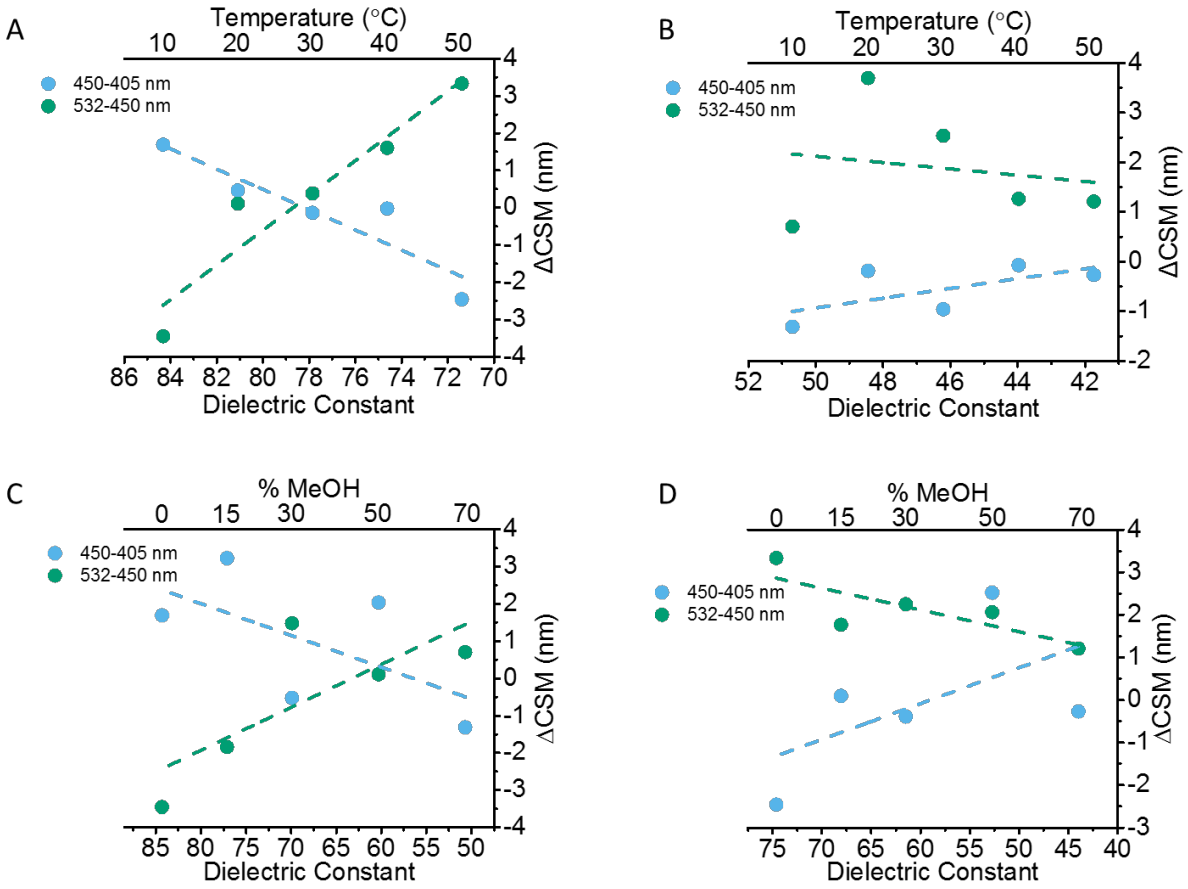

Figure 2. Variation in CSM of Alexa 488 *versus* change in dielectric constant of solvent where dielectric is changed by (**A** (0% MeOH), **B** (70% MeOH)), temperature or (**C** (10 °C), **D** (50 °C)) methanol concentration. Alexa 488 emission was measured in water and methanol/water mixtures at 405, 450, and 532 nm. The laser lines were subtracted from the spectra, and a skewed Gaussian was fit to the data. CSM values were calculated from the fitted emission spectra. The difference was then taken between the CSMs of 450 and 405 nm, and 532 and 450 nm to give ΔCSM. The dashed-lines are to aid the eye only.

to the formation of sub-visible aggregates and we corroborate this finding below. We note that a recent study has shown that a red edge-shift is observed on aggregation of κ-casein as it forms amyloid fibrils, based on tryptophan emission.[22] The edge-shift phenomenon is sensitive to changes in the dipole moment of the environment and so we suggest that whether a red or blue shift is observed is based in large part on the specifics of the aggregation type and environment, which controls the dipole moment of the fluorophore. We explore this in more detail below.

Excitation energy-dependent spectral shifts are most commonly observed as a red-shift in emission spectra, though blue-shifts have been previously characterized.[20] Therefore, we turned to free fluorophore solution studies using laser-based excitation to confirm the blue-shift we observe in Figure 1B is responsive to environmental relaxation (Figure 1A), i.e. that it is a bone fide excitation-energy-dependent edge-shift. Figure S3A-B shows that Alexa 488, free in buffered solution, gives both a blue- and a red-shift with increasing excitation wavelength. Figure S3C-E shows that these shifts are not attributable to the differential absorption of the excitation light at different excitation wavelengths, and are not due to the bandwidth of the excitation.

Edge-shift phenomena are based on slow dipolar relaxation of the solvent environment. Therefore, altering the solvent dipole should induce a change in the observed excitation energy-dependent edge-shift. Given the potential to observe either a red or a blue shift in excitation energy dependent fluorescence emission, we have conducted solvent studies to determine the dependence of a fluorophore on changes in environment (dielectric). We altered the solvent dipole by two independent methods, through varying methanol concentration and temperature, and the resulting effect on the observed edge-shift from Figure S3A/B is shown in Figure 2A-D. When using 0 % methanol, the dielectric constant was reduced through increasing temperature, and was found to give a blue-shift for the ΔCSM values of 450 and 405 nm. A red-shift was observed for 532 and 450 nm (Figure 2A). However, when changing the solvent system for 70 % methanol, a red-shift was observed for the ΔCSM of 450 and 405 nm, and a blue-shift for 532 and 450 nm (Figure 2B). At 10 and 50 °C, the dielectric constants were decreased by increasing methanol concentration. When measuring the ΔCSMs at 10 °C, a blue- shift was observed for 450 and 405 nm, and a red-shift for 532 and 450 nm (Figure 2C). This trend was inverted when the

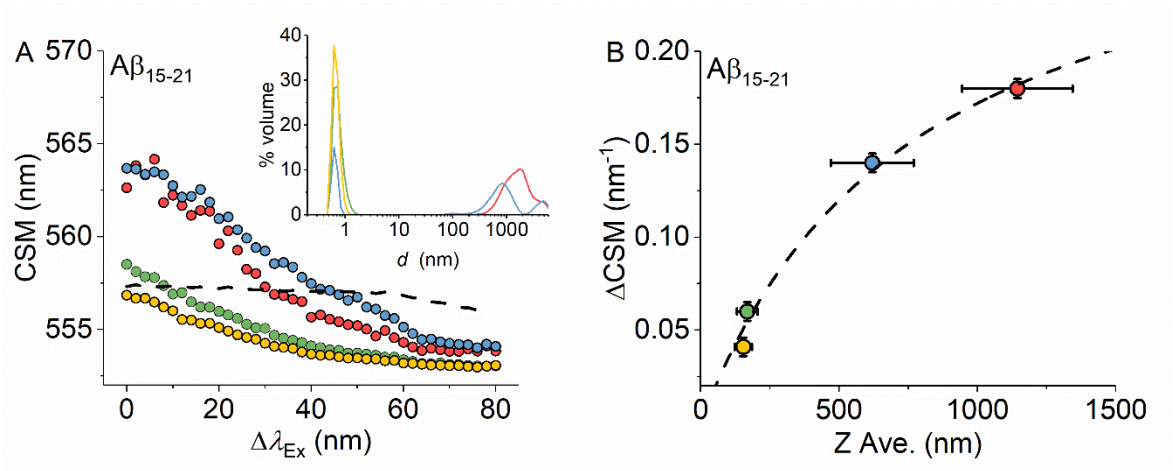

Figure 3. A, Edge-shift measurements demonstrating sensitivity between monomerized and aggregated states (shown as differently colored data points) of fluor-A$\beta_{15\text{-}21}$ and coloration is correlated between main panel and *inset*. The black dashed-line shows the data for fluorescein alone. *Inset,* DLS data for monomerized and aggregated fluor-A$\beta_{15\text{-}21}$. Coloration corresponds to aggregation state shown in *inset.* **B**, Correlation between the change in CSM (ΔCSM) for fluor-A$\beta_{15\text{-}21}$ shown in Panel A. The Z-average hydrodynamic diameter from the DLS data shown in Panel A. Coloration is as Panel A.

temperature was increased to 50 °C, showing a red-shift and blue-shift for ΔCSMs of 450 and 405 nm, and 532 and 450 nm, respectively (Figure 2D). The dielectric constants of the methanol/water mixtures were calculated as described by Andrenko and Wang[23] and correlated with the experimental data by Gosting and Albright.[24]

We find that both the blue- and red-shift (Figure S3E) are sensitive to changes in the dielectric constant of the solvent (Figure 2A-D). Figure S4 shows that these shifts are not due to differences in the absorption spectrum when varying methanol concentrations. From Figure 2, decreasing the dielectric constant gave rise to an inversion of the blue- and red-shifts. That is, the observed blue-shift becomes a red-shift and the observed red-shift becomes a blue-shift. These data are convincing evidence that the two edge-shifts arise from the same physical phenomenon, i.e. excitation-energy-dependent fluorescence edge-shift, as shown in Figure 1A. Moreover, these data suggest that a plausible mechanism for the large blue-shift, associated with the protein aggregation we observe above, are differences in the dipolar relaxation of the environment around the fluorophore on aggregate formation. We suggest this is because the early-stage aggregates are potentially amorphous, and the molecular beacon experiences a range of different molecular (dipolar) environments. This would explain the relative insensitivity to larger, structured aggregates that are essentially a homogenous repeating unit. Moreover, these data suggest that the same fluorophore can experience either a red or blue shift depending on changes in the local dielectric and this finding validates our finding of a blue edge-shift on protein aggregation (Figure 1B) and the observation of a red-shift for a different protein and fluorophore combination. We stress that our analysis does not at this point allow us to definitively assign the morphology and structure of aggregates, simply that we are detecting sub-visible aggregates.

Having established that the observed edge-shift is bone fide and provides a measurement of the presence of sub-visible protein aggregates in the mAb model systems, we sought to apply the approach to a biomedically important system where the formation of small soluble aggregates are relevant. Therefore, we synthesized the peptide fragment of Aβ that is responsible for the formation of toxic aggregates of the protein, A$\beta_{15\text{-}21}$ (QKLVFFA). This peptide has previously been used as a model for the full length Aβ[25] and has some advantages in the tractability of synthesis. The peptide was synthesized with an N-terminal fluorescein (fluor-A$\beta_{15\text{-}21}$) to monitor the change in edge-shift on aggregation of the peptide. We opted for the fluorescein label since labelling large quantities of peptide with Alexa 488 would be prohibitively expensive for most researchers, and we would like others to be able to adopt this approach.

Figure 3A shows the observed edge-shift for monomerized and aggregated fluor-A$\beta_{15\text{-}21}$ peptides and the corresponding raw emission and excitation spectra are shown in Figure S5A/B and S5C, respectively. Peptide aggregates were obtained by ageing the monomerized sample at room temperature and then separation by FPLC. Similar to the mAbs studied above, the excitation spectra essentially overlay at all emission wavelengths for the monomeric and aggregated protein (Figure S5C). Figure 3A inset shows the corresponding DLS profiles, showing the relative aggregation state of the samples. The ability of fluor-A$\beta_{15\text{-}21}$ to form amyloid-like fibrillar aggregates is confirmed by the binding of thioflavin-T (ThT), giving an increase in ThT emission (Figure S6).[26] However, we note that the aggregates we observe e.g. in Figure 3 are small and we suggest pre-fibrillar as we discuss below. Similar to the monomeric mAbs labelled with fluorescein, we observe a significant blue-shift associated with the monomeric fluor-A$\beta_{15\text{-}21}$. However, again similar to the fluorophore labelled mAb, the absolute magnitude of the edge-shift is small for the monomer (0.04 nm/nm) compared to the aggregated peptide (0.11 nm/nm).

Figure 3B shows the correlation between the absolute magnitude of the observed edge-shift versus the change in

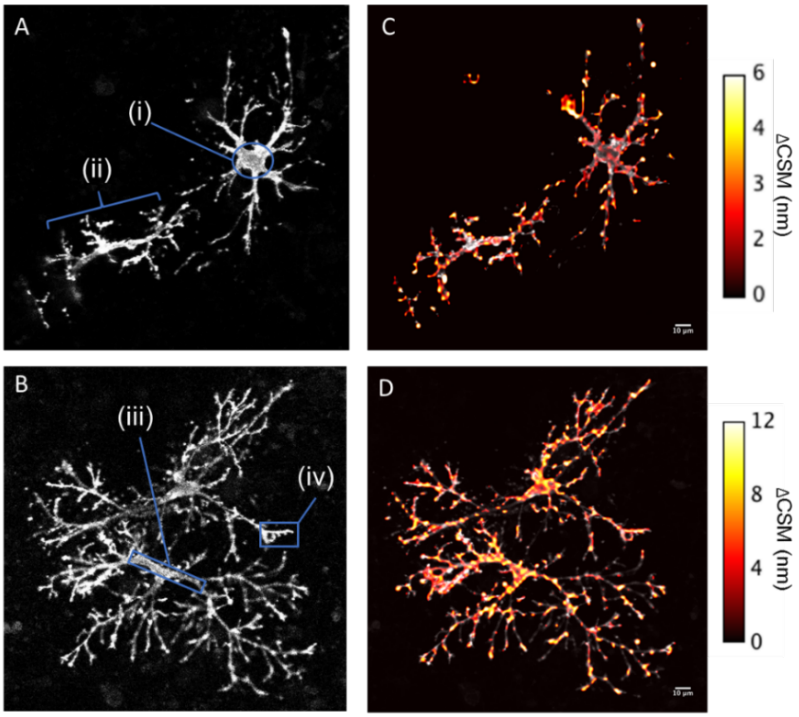

Figure 4. Mouse cortical neurons ('Cell 1', Panel A and 'Cell 2', Panel B) treated with 500 nM $A\beta_{15-21}$-fluor, analyzed by high resolution fluorescence microscopy. Labels i-iv show specific morphological features, likely corresponding to the cell body (i), dendrite (ii) periaxonal region (iii) and synapses (iv). C and D show the corresponding false color map of ΔCSM = CSM $\lambda_{Ex514nm}$ - CSM $\lambda_{Ex458nm}$ extracted from emission spectra of each image.

the intensity weighted aggregate size for fluor-$A\beta_{15-21}$. These data suggest, similar to the mAb data in Figure 1B that the magnitude of the edge-shift increases with the fraction of protein aggregate, but saturates as the aggregates tend towards visible (>1 μm). From Figure 3B it appears the edge-shift is most sensitive to relatively small aggregates, with highest sensitivity to hydrodynamic diameters on the low nanometer range (Figure 3A, inset). Such a size would correspond to low *n* oligomers of fluor-$A\beta_{15-21}$ ~ 10-100 mers, similar to the approximate size with the mAbs above (Figure 1B). We note that centrifugation does not yield a measureable pellet. The blue-shift appears to saturate(Figure 3B) as the aggregates approach visible sizes (Figure 3A inset), suggesting that the approach is insensitive to large (> 1 μm) aggregates that are classically captured by ThT assays. We suggest the reason for this insensitivity is because the late-stage fibrillar form of Aβ is essentially a homogenous repeating unit, and the edge-shift phenomenon is based on detecting sample heterogeneity where discrete states can be photo-selected. The sensitivity to the earliest stages of Aβ aggregates is important since it is the early stage aggregates that are considered to be the toxic species in AD.[3] Again we stress that at present we cannot definitively determine the aggregation morphology (e.g fibrillary or not) based on the edge-shift value, simply the overall hydrodynamic diameter.

Having established that the observed edge-shift can be used to track sub-visible protein aggregates, and that are relevant to Aβ toxicity, we wished to ask if edge-shift could be observed and quantified using a microscope platform and applied to cell studies. We cultured mouse primary cortical neurons (reflecting a key region of the brain affected by AD) for 7 days[27] and incubated the differentiated cells for 24 hours with a concentration of fluor-$A\beta_{15-21}$ that is within the range typically used for pathophysiological studies in vitro (500 nM).[28] The presence of fluor-$A\beta_{15-21}$ gave rise to significant morphological changes to the neurons, potentially indicative of neuro-toxicity as expected (Figure S7). The neurons were then washed with phosphate buffered saline (PBS) to remove non-bound fluor-$A\beta_{15-21}$ and fixed with 4% paraformaldehyde. Paraformaldehyde does not affect the absolute magnitude of the observed edge-shift giving, 0.039 nm/nm and 0.036 nm/nm for the untreated and paraformaldehyde treated fluor-$A\beta_{15-21}$, respectively.

Figures 4A (Cell 1) and 2B (Cell 2) show examples of neurons with different morphologies. Cell 1 shows a large discrete cell body, proximal axons, and a dendritic network. Cell 2 shows a much more extensive and elaborate dendritic network, allowing better quantification of the edge-shift with respect to synaptic localization. We note that these assignments are based on the morphology of the cells and not confirmed by cell marker staining, due to the concern that introducing another dye molecule may affect the emission characteristics of the fluor-$A\beta_{15-21}$ through either resonance energy transfer (RET) or direct collisional

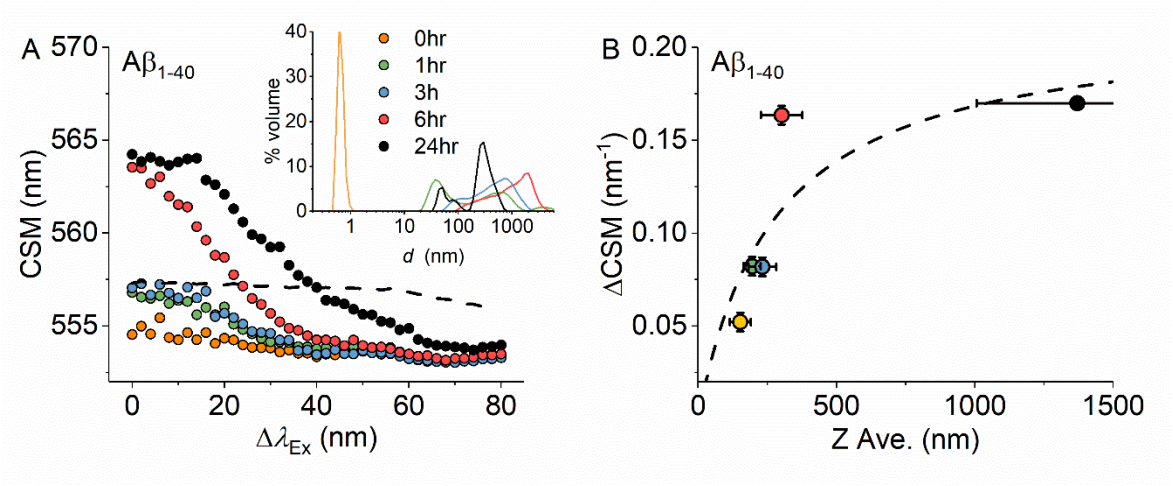

Figure 5. A, Edge-shift measurements demonstrating sensitivity between monomerized and aggregated states of fluor-Aβ$_{1\text{-}40}$ that have been aged for different time periods (*inset*) at 25 °C. The black dashed-line shows the data for fluorescein alone. *Inset,* DLS data for monomerized and aggregated fluor-Aβ$_{1\text{-}40}$. Coloration corresponds to time points in *inset*. **B**, Correlation between the change in CSM (ΔCSM) for fluor-Aβ$_{1\text{-}40}$ shown in Panel A. The Z-average hydrodynamic diameter from the DLS data shown in Panel A. Coloration is as Panel A.

quenching. At present we are not aware of any study that details the optical physics of such interactions relating specifically to edge-shift phenomena and so we have been reluctant to convolve the present data set with this unknown. That said, our study aims to illustrate the potential of the approach and to establish the routes to and limitations of its use.

To extract the cellular CSM versus λ_{Ex} profile, we monitored the EEM spectra of the fixed cells using a Leica SP8 confocal microscope with spectral detection across the excitation range of 405-514 nm. Figures 4C and 4D show the processed EEM data to give the absolute magnitude of the blue-shift as the difference in CSM between λ_{Ex} 458 and 516 nm, and were overlaid as a false color image onto the corresponding fluorescence image from Figures 4A and 4B. CSMs were calculated on a per pixel basis after smoothing with a Gaussian filter with a 6 pixel FWHM diameter. The coloration is based on the absolute magnitude of the observed blue-shift. The control experiment with fluorescein imaged alone is shown in Figure S8, giving a total edge-shift of ~1 nm between λ_{Ex} 458-516 nm. From Figure 4C and 4D, we find that the magnitude of the blue-shift varies significantly depending on the cellular morphology. Zoomed in views of the subcellular regions in Figure 4A and 4B are shown in Figure S9.

The cell body evident in Figure 4A shows essentially no edge-shift, consistent with the measurement from fluorescein alone (Figure S9). A larger edge-shift is observed for the axons and dendrites in both Figure 4C and 4D (Figure S9). Without staining it is difficult to definitively identify synaptic structures. However, in many cases we find that the likely locations of synapses and terminals, based on morphology, is coincident with very high magnitudes of measured edge-shift (Figure S9). Indeed, we selected Cell 2 because of its extensive dendritic network where we anticipate a large number of synapses will be located. Cell 2 shows a globally larger edge-shift compared to Cell 1, which has a rather less developed dendritic structure. From Figure 3 we find that, for fluor-Aβ$_{15\text{-}21}$, an increase in the blue-shift is commensurate with the formation of sub-visible, aggregates. Therefore, the data in Figure 4 suggest that formation and association of early-stage fluor-Aβ$_{15\text{-}21}$ aggregates are dependent on the cellular environment. Potentially these toxic species associate with dendrites but again we note the caveat of assigning sub-cellular structures based on morphology. This putative finding would however be consistent with the proposed synaptic binding sites and receptors for Aβ in neurons.[29] The large magnitude edge-shift values do not necessarily correlate with large fluorescence intensity readings in Figure 4, as shown in Figure S9. That is, the extracted edge-shift values are not representing high local concentrations of the fluor-Aβ$_{15\text{-}21}$, but more specifically capturing differences in early-stage aggregation state. Given the potential demonstrated with the fluor-Aβ$_{15\text{-}21}$ we next examined a similar data-set with a longer form of Aβ, fluor-Aβ$_{1\text{-}40}$ as shown in Figures 5-7

Figure 5 shows the observed edge-shift for the fluor-Aβ$_{1\text{-}40}$ 40 peptide but now aged over 24 hours at 25 °C, starting from the monomerized fluor-Aβ$_{1\text{-}40}$. The corresponding raw excitation/emission spectra are shown in Figure S10. Figure 5A, inset shows the corresponding DLS profiles and Figure 5B shows the correlation between the observe edge-shift and the size of aggregate. From Figure 5 the blue shift we observe with fluor-Aβ$_{15\text{-}21}$ is essentially recapitulated for fluor-Aβ$_{1\text{-}40}$ and even the relationship of aggregate size to the magnitude of edge-shift is qualitatively very similar (c.f. Figures 3B and 5B). We note that none of the time points we have tested show any significant emission arising from ThT binding (Figure S11) suggesting that, as with fluor-Aβ$_{15\text{-}21}$ above, the edge-shift is only sensitive to the early-stage aggregates of Aβ. Moreover, similar to fluor-Aβ$_{15\text{-}21}$, we find that the magnitude of the edge shift

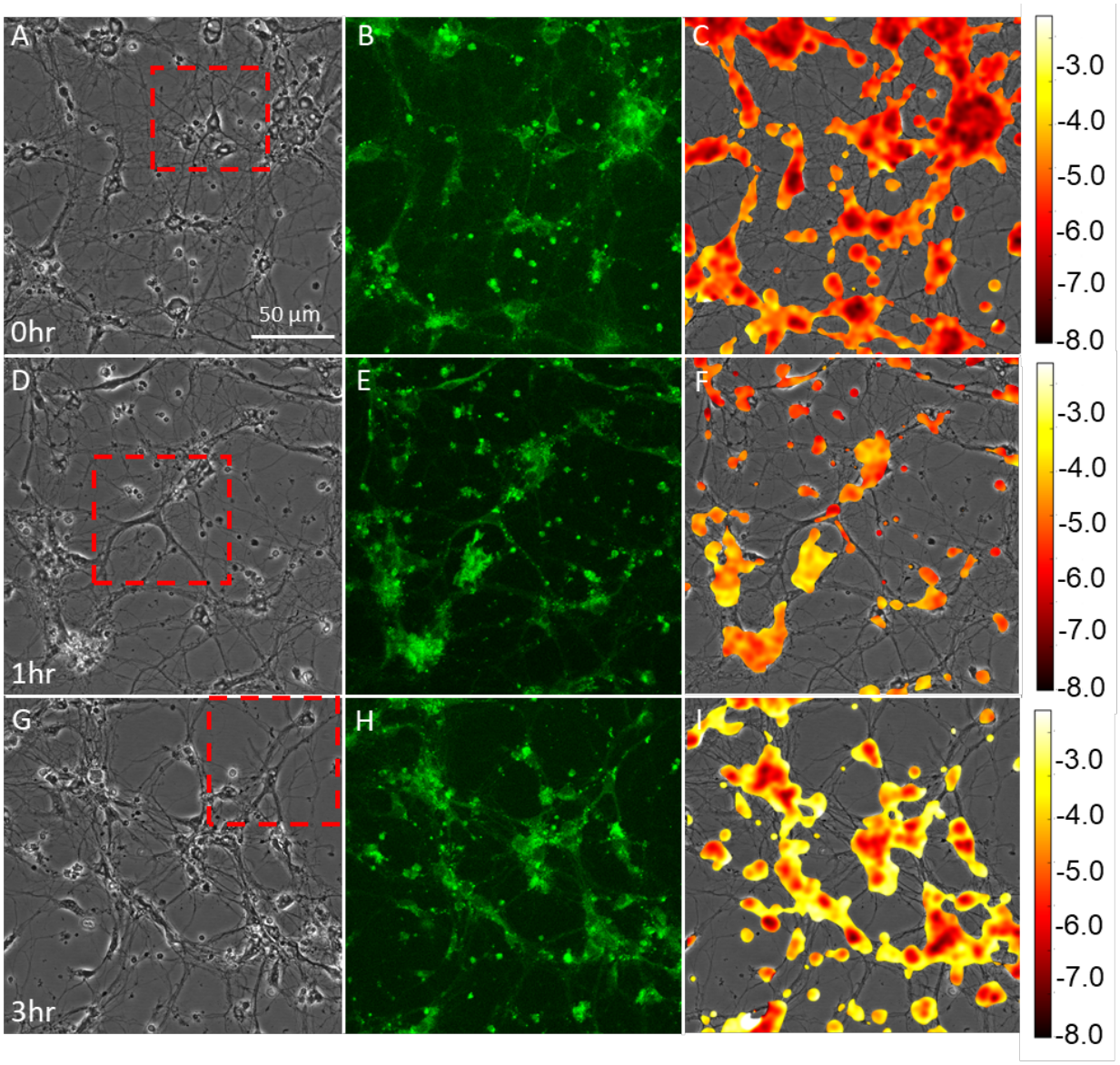

Figure 6. Mouse cortical neurons treated with aged 500 nM fluor-$A\beta_{15-21}$ from Figure 5 at 0 hr (A), 1 hr (D) and 3 hrs (G). The panels at right of each condition show a corresponding fluorescence emission image ($\lambda_{Ex458nm}$; panels B, E and H) and the extracted edge shift value ($\lambda_{Ex514nm}$ - CSM $\lambda_{Ex458nm}$; panels C, F, and I) overlaid as a false color map the corresponding image (panel A, D and G). The scale bar at right corresponds to the ΔCSM values in the edge-shift false color maps.

saturates as the hydrodynamic diameter approaches ~1 µm (Figure 5B). Finally, from Figure S12, we show that fluor-$A\beta_{1-40}$ is cytotoxic (based on MTT absorption to assess cytotoxicity) as one expects and compared to a scrambled version of fluor-$A\beta_{15-21}$ (fluor-FKFQVAL), which does not show any significant edge-shift and is not predicted to aggregate based on sequence analysis.

We have imaged 500 nM fluor-$A\beta_{1-40}$ in the presence of cortical neurons as in Figure 4, but using the fluor-$A\beta_{1-40}$ samples aged as in Figure 5. The resulting data for 0, 1 and 3 hours are shown in Figure 6. At 6 and 24 hours we observed only sparse fluorescence emission and we have not analysed the edge shift values for these data as we were not confident that the signal magnitude would allow us to extract accurate CSM values. From Figure 6 there is clearly association of fluor-$A\beta_{1-40}$ with the neurons as with fluor-$A\beta_{15-21}$ in Figure 4. The magnitude of edge-shift is similar as with fluor-$A\beta_{15-21}$, but now is red-shifted c.f. blue-shifted. The observed red edge-shift is also in contrast with the solution studies with fluor-$A\beta_{1-40}$ (Figure 5), where a blue-shift is observed on aggregation. As with fluor-$A\beta_{15-21}$ the large magnitude edge-shift values do not necessarily correlate with the highest intensity fluorescence regions. This confirms that the absolute magnitude of emission is not a good reporter of early stage aggregate association on cells. We note that the scrambled fluor-$A\beta_{15-21}$ peptide shows hardly any emission under the same incubation times with the same cultured neurons (Figure S13) and is insufficient to generate a similar false color map of the edge-shift as in Figure 6. These data suggest that the observed edge shift in the presence of cultured neurons is not significantly convolved of non-specific binding.

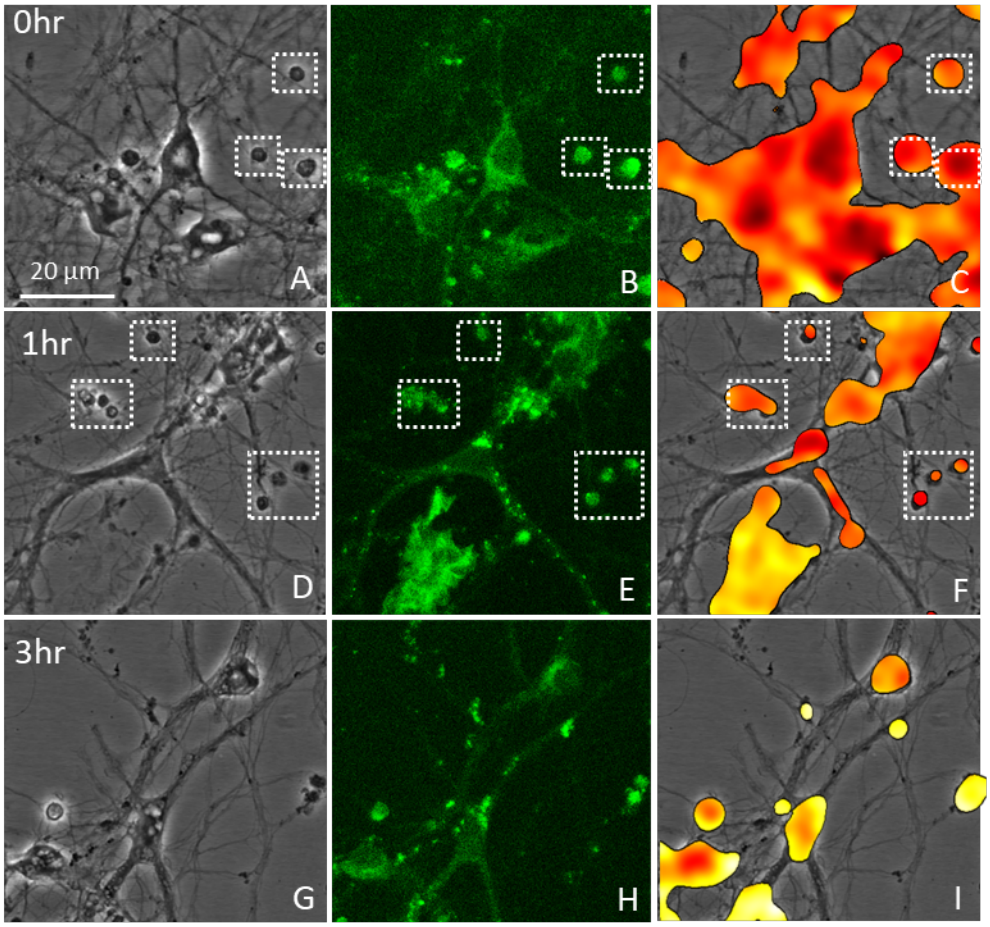

Figure 7. Expanded view of images in Figure 6 (red dashed boxes). Panels correspond to the counterpart in Figure 6. Edge-shift scale bars are as in Figure 6. Cellular features discussed in the main text are highlighted with white dashed boxes.

The local concentration of fluor-A$\beta_{1\text{-}40}$ may be highly variable depending on association with sub-cellular features and aggregation state. We do not find a significant change in the magnitude of the edge-shift value associated with different concentrations of the monomerised fluor-A$\beta_{1\text{-}40}$ (Figure S14), suggesting the observed changes in edge-shift shown in Figure 6 are not artifacts arising from changes in local concentration.

We have also attempted to monitor the signal arising from fluor-A$\beta_{1\text{-}40}$ aged in the presence of cells, however we found that the emission signal dissipated after 1 hr. Recent evidence has suggested that apoptosis-associated speck-like protein containing a CARD (ASC) specks released by microglia, formed on Aβ deposition, increases the formation of Aβ oligomers and aggregates.[30] Potentially, the partially aggregated fluor-A$\beta_{1\text{-}40}$ from Figure 5 gives improved binding in the first instance, at least under the conditions reported. A potential hypothesis therefore is that the sample aged in the presence of neurons are not induced to form aggregates because of a lack of ASC specks.

The observation of a red versus a blue edge-shift is readily explained from our model fluorophore studies shown in Figure 2 and described above. These data show that a blue shift can transition to a red-shift, purely based on changes in solvent (environment) dielectric constant and this is consistent with the expected physical interpretation of edge shift phenomenon. Specifically, for the corresponding wavelength range studied in Figures 5, the data in Figure 2 suggest a red shift occurs as the dielectric of the environment becomes smaller. That is, in the presence of neurons, the fluorophore molecular beacon is located in a relatively high dielectric environment for fluor-A$\beta_{15\text{-}21}$ aggregates and in a relatively low dielectric environment for fluor-A$\beta_{1\text{-}40}$ aggregates.

The dielectric constant inside a protein is generally much lower than at the proteins surface[31] and so our data suggest the fluorophore molecular beacon is buried in protein aggregates for fluor-A$\beta_{1\text{-}40}$ and rather more solvent exposed for fluor-A$\beta_{15\text{-}21}$. Indeed, recent studies using tryptophan as an intrinsic reporter of protein aggregation find a red edge-shift,[22] corroborating this notion. Taken together, our finding of a red shift for fluor-A$\beta_{1\text{-}40}$ in the presence of cells versus a blue-shift in solution potentially suggests an aggregate conformation (dipole environment) that is unique to the combination of fluor-A$\beta_{1\text{-}40}$ and the cellular microenvironment. That we find a different aggregate conformation in the presence of neurons versus buffered solution suggests a hypothesis where the cellular environment drives a specific aggregation mechanism that is unique to the full length Aβ. We would stress that this represents a working

hypothesis, since only a discrete whole cell study could confidently validate the hypothesis. However, we believe these data are intriguing and provide the rationale for the exploration of the hypothesis.

Membrane association has the potential to alter the environmental relaxation rate of the fluorophore.[32] Therefore, we wished to test if the immediate sub-cellular environment is the origin of the edge-shift observed for Aβ1-40, instead of a specific conformational state of the aggregate. We have therefore incubated fluor-$A\beta_{1-40}$ with nanodiscs, similar to previous studies[33] and observed the edge-shift at zero and six hours as shown in Figure S15. From Figure S15 we find the presence of the membrane environment has only a small effect on the magnitude of the observed edge shift and is trivial compared to the magnitude of the edge-shift attributable to Aβ aggregation. Most importantly we do not observe that the presence of the membrane induces a red-shift in the data and so the observed red-shift for fluor-$A\beta_{1-40}$ in the presence of cells is not a consequence of membrane association. That is, the membrane environment itself does not drive the aggregation inferred from the edge-shift data. It would seem likely this is driven by specific and possibly multiple protein-protein interactions. For example, the recent finding that ACS specks promote aggregate formation as discussed above. Potentially, the approach described here could be a useful platform to screen for important protein-protein interactions that give rise to Aβ aggregate binding and internalization.

The time course study shown in Figure 6 reveals further details on the relationship between aggregate formation and localization. At 0 hrs (Figure 5A-C) there is a large edge-shift, which is diffusely spread across essentially all of the cells and sub-cellular features These data suggest the neurons induce relatively rapid aggregation of fluor-$A\beta_{1-40}$ (on the time-scale of preparation of the cells; ~minutes). At subsequent time points (1 hr, Figures D-F; 3 hrs, Figures G-I), the location of the aggregates becomes increasingly less diffuse and more localized, becoming almost entirely associated with putative cell soma with some discrete punctate labeling evident in putative axonal and peri-axonal regions (based on morphology as above), shown in the expanded images in Figure 7. Indeed, it is the putative soma, in all cases, that appears to be coincident with the largest edge-shift value and the other sub-cellular environments (axons, dendrites) have little to no edge-shift. We note that the absolute fluorescence intensity at each time point is similar (Figure 6). These data therefore potentially suggest that over time, early-stage Aβ aggregates are internalized in the soma or rapidly trafficked to the cell soma. These findings are in stark contrast to the findings with the fluor-$A\beta_{15-21}$ (Figure 4), where the soma appears to be relatively free of aggregates, and the association is primarily with the axons/dendrites. Most importantly, these data very clearly illustrate the critical importance of considering both a full-length Aβ peptide and in the presence of an appropriate cellular model when attempting to study early-stage Aβ aggregation. We would stress that we are cautious in this interpretation of the results, not least because we cannot yet apply both the edge shift approach and cell staining as described above (though we anticipate this will be possible in the future). The most important finding from our data is that the edge shift value varies depending on sub-cellular location and appears to be linked to aggregation state. Clearly, there is a great deal of further work required but the present study points to the potential utility of this approach.

Finally, the data in Figures 6 and 7 show an intriguing correlation between very large edge-shift values (progressed aggregation) and distinct cellular features that are not readily identifiable based simply on their morphology. Examples are highlighted in Figure 7 (white dashed boxes). These structures potentially represent shrunken cell bodies consistent with labeling of apoptotic cell corpses. The co-localisation of highly aggregated Aβ with these features points to an important cellular context in which further studies could fruitfully be applied using the edge-shift approach to probe the mechanisms of Aβ induced neuronal cell death.

CONLUSIONS

We have demonstrated the edge-shift in the emission spectra of fluorophore labeled proteins can report on very early stage (sub-visible) aggregates. We have applied this finding to whole-cell microscopy experiments to monitor the formation of early-stage toxic aggregates of Aβ, at physiological concentrations, in mouse primary cortical neurons. We find that the edge-shift is readily observable in the presence of a relevant cell type, and that the additional information from the microscopy platform potentially allows site specific measurement of the magnitude of the edge-shift. Based on these preliminary studies, our data prompts the hypothesis that Aβ aggregation occurs in a site-specific manner on neuronal cells and that the neurons themselves, or their local environment, potentially drive the formation and specific conformation of the aggregates. We note that, at present, no other approach that we are aware of is able to detect and quantify these sub-visible aggregates on a microscopy platform using whole-cells, with a sensitivity that can detect differences in subcellular location.

Clearly, a caveat with the approach is that it relies on labelling the protein of interest. Therefore, while we do not advocate this approach for diagnostic imaging, our findings point the way for studying the underlying cause of Aβ pathology in AD as well as other neurotoxic protein aggregates. Moreover, our study suggests the absolute magnitude of the edge-shift will be sensitive to (i) aggregate size, (ii) distribution of different aggregates and (iii) morphology of the aggregates. Disentangling these contributions is the next step in developing the utility of this approach and our data point to the potentially very high discriminatory power. A part of this understanding will come from detail photo-physical studies of the edge-shift phenomenon itself. Finally, we see high potential for imaging at the super-resolution level combined with bio-orthogonal labelling strategies to explore different cellular contexts in fine detail. That is, we suggest that building the edge-shift ap-

proach into other detection methodologies will significantly enhance the utility of the methods used in isolation. Given that the edge-shift approach has the advantage that it does not require specialist instrumentation, and uses established, readily available fluorescent probes we anticipate this should be an achievable goal in the short term.

EXPERIMENTAL PROCEDURERS

Antibody Labelling. Antibodies (Rituximab and Nivolumab) were a kind gift from Bath ASU (Corsham, UK). Antibodies were labelled with Alexa Fluor® 488 C5-Maleimide from Molecular Probes by Life Technologies or Fluorescein-5-Maleimide from Thermo Scientific. To 1 mL of 50 mM Tris-HCl pH 8.0 buffer, 50 μL of antibody and 10 μL (10 mg/mL) of 14 mM (Alexa 488) or 47 mM (fluorescein-5-maleimide) dye were added and the mixture was left at 5 ˚C for 1 hour. The protein was then run through a PD-10 desalting column and the absorbance was measured on a Varian Cary 50 Bio UV-Visible spectrophotometer (Varian, Walnut Creek, CA, USA) to monitor antibody tagging. Aggregation was induced thermally for 30 minutes at 60 ˚C for Nivolumab and 70 ˚C for Rituximab. The antibodies were a kind gift from Bath ASU.

Dynamic Light Scattering (DLS). Aggregation data was obtained in a 50 μL quartz cuvette on a Malvern Zetasizer Nano S (Malvern, Worcestershire, UK) to determine hydrodynamic radius. Samples were left to equilibrate for 2 minutes at 25 ˚C then measured in triplicate and averaged for reporting.

Fluorescein Labelled Amyloid β Synthesis. Rink amide ChemMatrix™ resin was obtained from PCAS Biomatrix, Inc. (St.-Jean-sur-Richelieu, Canada); Fmoc l-amino acids and 2-(1H-benzotriazole-1-yl)-1,1,3,3-tetramethyluronium hexafluorophosphate or benzotriazol-1-yl-oxytripyrrolidinophosphonium hexafluorophosphate were obtained from AGTC Bioproducts (Hessle, UK); all other reagents were of peptide synthesis grade and obtained from Thermo Fisher Scientific (Loughborough, UK). Peptides were synthesized on a 0.1 mmol scale on a PCAS ChemMatrix™ Rink amide resin using a Liberty Blue™ microwave peptide synthesizer (CEM; Matthews, NC) employing Fmoc solid-phase techniques with repeated steps of coupling, deprotection and washing (4 × 5 mL dimethylformamide).[34] Coupling was performed as follows: Fmoc amino acid (5 eq), 2-(1H-benzotriazole-1-yl)-1,1,3,3-tetramethyluronium hexafluorophosphate or benzotriazol-1-yl-oxytripyrrolidinophosphonium hexafluorophosphate (4.5 eq) and diisopropylethylamine (10 eq) in dimethylformamide (5 mL) for 5 min with 35-W microwave irradiation at 90 °C. Deprotection was performed as follows: 20% piperidine in dimethylformamide for 5 min with 30-W microwave irradiation at 80 °C. Following synthesis, the peptide was labelled with 5(6)-carboxyfluorescein using a standard coupling step for 20 min—and then cleaved it from the resin with concomitant removal of side-chain-protecting groups by treatment with a cleavage mixture (10 mL) consisting of TFA (95%), triisopropylsilane (2.5%) and H2O (2.5%) for 4 h at room temperature. Suspended resin was removed by filtration, and the peptide was precipitated using three rounds of crashing in ice-cold diethyl ether, vortexing and centrifuging. The pellet was then dissolved in 1:1 MeCN/H2O and freeze-dried. Purification was performed by RP-HPLC using a Phenomenex Jupiter Proteo (C18) reverse-phase column (4 μm, 90 Å, 10 mm inner diameter × 250 mm long). Eluents used were as follows: 0.1%TFA in H2O (a) and 0.1% TFA in MeCN (b). The peptide was eluted by applying a linear gradient (at 3 mL/min) of 5–70% B over 40 min. Fractions collected were examined by electrospray MS, and those found to contain exclusively the desired product were pooled and lyophilized. Analysis of the purified final product by RP-HPLC indicated a purity of > 95%. Prior to running fluorescence measurements, fluorescein labelled Aβ15-21 and Aβ1-40 were monomerized using Zagorski methodology, followed by size exclusion on a PD-10 column to separate monomerized and aggregated material.[35]

Fluorescence Measurements. REES measurements were carried out on a Perkin Elmer LS50B Luminescence Spectrometer (Perkin Elmer, Waltham, MA, USA) which was temperature regulated (±1 ˚C) using a circulating water bath. Samples were allowed 5 minutes to equilibrate prior to measurements. Measurements were obtained at 20 ˚C for labelled antibodies and 10 ˚C for fluorescein labelled amyloid β. Excitation-emission slits were 4.0 nm for Alexa 488 tagged antibodies and fluorescein tagged Aβ. Formaldehyde studies for fluorescein tagged Aβ used excitation-emission slit widths of 6.0 nm. Alexa 488 emission was measured from 480 to 620 nm, with excitation scans taken every 2 nm from 410 to 460 nm. Fluorescein emission was monitored from 535 to 650 nm, with excitation varied every 2 nm from 400 to 520 nm. All measurements were performed in triplicate with the corresponding buffers also measured and subtracted from the spectra for each sample.

For single wavelength excitation measurements, excitation sources were 4.5 mW laser diode modules (405, 450, 532 nm) and fluorescence emission was detected with a compact CCD CCS100 spectrometer (ThorLabs, Newton, NJ, USA).

The center of spectral mass (CSM) was calculated using:

$$\mathrm{CSM} = \frac{\sum(fi_i \times \lambda_{Em})}{\sum(fi_i)} \qquad \text{Eq 1}$$

where the measured fluorescence intensity is fi and the emission wavelength is λ_{Em}. For measurements in buffered solution the concentration of protein/peptide used was typically between 1-2 μM and for microscopy experiments with neurons present, the concentration was 500 nM (buffer in both cases is PBS).

High Resolution Fluorescence Microscopy. REES measurements were carried out on a Leica SP8 confocal microscope, Leica Microsystems with an Argon ion laser as the excitation source for 458, 476, 488, 496, and 514 nm with total power of 65 mW. A 50 mW diode laser was used for λEx measurements at 405 nm. Measurements were carried out at 37 ˚C measuring emission from 542.5 to 638.5 nm. As 405 nm gave a high amount of autofluorescence, CSM values were calculated for cells from 458 nm upward where

there is effectively no autofluorescence to be convolved in the signal.

Primary Neuronal Cell Culture. Primary cortical neurons were prepared from CD1 mouse embryos in accordance with UK Home Office Guidelines as stated in the Animals (Scientific Procedures) Act 1986 using Schedule 1 procedures approved by the University of Bath Animal Welfare and Ethical Review Body. Primary neurons were prepared essentially as described previously (22).Cortices were dissected from 15-day-old CD1 mouse embryos, and were mechanically dissociated in PBS supplemented with 33 mM glucose, using a fire-polished glass Pasteur pipette. Cells were plated into either 12- or 24-well Nunc tissue culture plates, previously coated with 20 µg/ml poly-D-lysine (Sigma). Neurons were cultured in Neurobasal medium (phenol red free) supplemented with 2 mM glutamine, 100 µg/ml penicillin, 60 µg/ml streptomycin and B27 (all from Invitrogen), and incubated at 37°C, in high humidity with 5% CO_2. Under these growth conditions at 7-8 days in vitro (DIV) cells had a well-developed neuritic network and were 99% β-tubulin III positive and <1% GFAP positive.

ASSOCIATED CONTENT

Supporting Information. Absorption, emission and excitation spectra corresponding to the EEM data shown, microscopy image showing whole cells and zoomed in views, scrambled peptide and nanodisc control experiments. This material is available free of charge via the Internet at http://pubs.acs.org.

AUTHOR INFORMATION

Corresponding Author

* To whom correspondence should be addressed: Dr Jody Mason, Dr Robert J. Williams and Dr Christopher R Pudney from the Department of Biology and Biochemistry, University of Bath, Bath, United Kingdom. E-mail: j.mason@bath.ac.uk, r.j.williams@bath.ac.uk and c.r.pudney@bath.ac.uk; Tel +44 (0)1225 385049.

Present Addresses

†If an author's address is different than the one given in the affiliation line, this information may be included here.

Author Contributions

CEG, RM, DA, DAMC, RJW conducted experiments. CEG, CS, DDJ, VKV, GDP, JMM, RJW and CRP designed experiments. All authors interpreted data and contributed to data analysis. All authors wrote the manuscript. All authors have given approval to the final version of the manuscript.

Funding Sources

This work was supported by grants from the EPSRC, the GW4 University Alliance and BBSRC Alert 13 capital grant (BB/L014181/1) funding the Wolfson Bioimaging Facility.

ACKNOWLEDGMENT

The mAbs used were a kind gift from Bath ASU, Corsham, UK.

ABBREVIATIONS

Aβ, Amyloid-β protein; AD, Alzheimer's disease; CSM, center of spectral mass; EEM, excitation/emission matrix; REES, red-edge excitation-shift; mAb, monoclonal antibody; RET, resonance energy transfer.

REFERENCES

1. De Strooper, B., and Karran, E. (2016) The Cellular Phase of Alzheimer's Disease. *Cell. 164*, 603–615
2. Ferreira, S. T., Lourenco, M. V, Oliveira, M. M., and De Felice, F. G. (2015) Soluble amyloid-β oligomers as synaptotoxins leading to cognitive impairment in Alzheimer's disease. *Front. Cell. Neurosci. 9*, 191
3. Viola, K. L., and Klein, W. L. (2015) Amyloid β oligomers in Alzheimer's disease pathogenesis, treatment, and diagnosis. *Acta Neuropathol. 129*, 183–206
4. Lee, J., Culyba, E.K., Powers, E.T. & Kelly, J.W. (2011) Amyloid-beta forms fibrils by nucleated conformational conversion of oligomers. *Nat Chem Biol 7,* 602-609
5. Xu, M., Ren, W., Tang, X., Hu, Y., and Zhang, H. (2016) Advances in development of fluorescent probes for detecting amyloid-β aggregates. *Acta Pharmacol. Sin. 37*, 1–12
6. Young, L. J., Kaminski Schierle, G. S., & Kaminski, C. F. (2017) Imaging Ab(1–42) fibril elongation reveals strongly polarised growth and growth incompetent states. *Phys. Chem. Chem. Phys. 19*, 27987.
7. Hatai, J., Motiei, L., & Margulies, D. (2016) Analyzing Amyloid Beta Aggregates with a Combinatorial Fluorescent Molecular Sensor. *J. Am. Chem. Soc. 139*, 2136-2139.
8. Horrocks, M. H., Lee, S. F., Gandhi, S., Magdalinou, N. K., Chen, S. W., Devine, M. J., Tosatto, L., Kjaergaard, M., Beckwith, J. S., Zetterberg, H., Iljina, M., Cremades, N., Dobson, C. M., Wood, N.W., & David Klenerman, D. (2016) Single-Molecule Imaging of Individual Amyloid Protein Aggregates in Human Biofluids. *ACS Chem. Neurosci.7*, 399-406.
9. Nag, S., Chen, J., Irudayaraj, J., & Maiti, S. (2010) Measurement of the Attachment and Assembly of Small Amyloid-b Oligomers on Live Cell Membranes at Physiological Concentrations Using Single-Molecule Tools. *Biophys. J. 99*, 1969–1975.
10. Demchenko, A. P. (2002) The red-edge effects: 30 years of exploration. *Luminescence. 17*, 19–42
11. Itoh, K. (1975) Shift of the emission band upon excitation at the long wavelength absorption edge. II. Importance of the solute–solvent interaction and the solvent reorientation relaxation process. *J. Chem. Phys. 62*, 3431-3438.
12. Azumi, T., Itoh, K., and Shiraishi, H. (1976) Shift of emission band upon the excitation at the long wavelength absorption edge. III. Temperature dependence of the shift and correlation with the time dependent spectral shift. *J. Chem. Phys. 65*, 2550–2555
13. Demchenko, A. P., and Ladokhin, A. S. (1988) Red-edge-excitation fluorescence spectroscopy of indole and tryptophan. *Eur. Biophys. J. 15*, 369–379
14. Chattopadhyay, A., and Haldar, S. (2014) Dynamic insight into protein structure utilizing red edge excitation shift. *Acc. Chem. Res. 47*, 12–19
15. Catici, D. A. M., Amos, H. E., Yang, Y., van den Elsen, J. M. H., and Pudney, C. R. (2016) The red edge excitation shift phenomenon can be used to unmask protein structural ensembles: implications for NEMO–ubiquitin interactions. *FEBS J. 283,* 2272-2284
16. Chattopadhyay, A., Rawat, S. S., Kelkar, D. A, Ray, S., and Chakrabarti, A. (2003) Organization and dynamics of tryptophan residues in erythroid spectrin: novel structural features of denatured spectrin revealed by the wavelength-selective fluorescence approach. *Protein Sci. 12*, 2389–2403

17. Kelkar, D. A., Chaudhuri, A., Haldar, S., and Chattopadhyay, A. (2010) Exploring tryptophan dynamics in acid-induced molten globule state of bovine α-lactalbumin: A wavelength-selective fluorescence approach. *Eur. Biophys. J. 39*, 1453–1463

18. Demchenko, A. P., and Sytnik, A. I. (1991) Solvent reorganizational red-edge effect in intramolecular electron transfer. *Proc. Natl. Acad. Sci. U. S. A. 88*, 9311–9314

19. Haldar, S., Chaudhuri, A., and Chattopadhyay, A. (2011) Organization and dynamics of membrane probes and proteins utilizing the red edge excitation shift. *J. Phys. Chem. B. 115*, 5693–5706

20. Nemkovich, N., Matseyko V. T. V. (1980) Intermolecular Up-Relaxation in Phthalimide Solutions at Excitation by Frequency Tuned Dye Laser. *Opt. Spectrosk. 49*, 274–283

21. Tjernberg, L. O., Näslund, J., Lindqvist, F., Johansson, J., Karlström, a R., Thyberg, J., Terenius, L., and Nordstedt, C. (1996) Arrest of beta-amyloid fibril formation by a pentapeptide ligand. *J. Biol. Chem. 271*, 8545–8548

22. Chakraborty, H., and Chattopadhyay, A. (2017) Sensing Tryptophan Microenvironment of Amyloid Protein Utilizing Wavelength-Selective Fluorescence Approach. *J. Fluoresc. 27*, 1995–2000

23 Wang, P. & Anderko, A. (2001) Computation of dielectric constants of solvent mixtures and electrolyte solutions. *Fluid Phase Equilibria 186*, 103–122

24 Albright, P. S. & Gosting, L. J. Dielectric Constants of the Methanol-Water System from 5 to 55°. *J. Am. Chem. Soc. 68*, 1061–1063 (1946).

25 Tjernberg, L. O., Callaway, D. J. E., Tjernbergi, A., Hahne, S., Lilliehook, C., Terenius, L., Johan Thyberg, J., & Nordstedt, C. (1999) A Molecular Model of Alzheimer Amyloid b-Peptide Fibril Formation. *J. Biol. Chem. 274*, 12619-12625.

26. Levine, H. (1993) Thioflavine T interaction with synthetic Alzheimer's disease β-amyloid peptides: Detection of amyloid aggregation in solution. *Protein Sci. 2*, 404–410

27. Cox, C. J., Choudhry, F., Peacey, E., Perkinton, M. S., Richardson, J. C., Howlett, D. R., Lichtenthaler, S. F., Francis, P. T., and Williams, R. J. (2015) Dietary (-)-epicatechin as a potent inhibitor of βγ-secretase amyloid precursor protein processing. *Neurobiol. Aging. 36*, 178–187

28. Abbott, J. J., Howlett, D. R., Francis, P. T., and Williams, R. J. (2008) $A\beta_{1-42}$ modulation of Akt phosphorylation via α7 nAChR and NMDA receptors. *Neurobiol. Aging. 29*, 992–1001

29. Shankar, G. M., Li, S., Mehta, T. H., Garcia-Munoz, A., Shepardson, N. E., Smith, I., Brett, F. M., Farrell, M. A., Rowan, M. J., Lemere, C. A., Regan, C. M., Walsh, D. M., Sabatini, B. L., and Selkoe, D. J. (2008) Amyloid-beta protein dimers isolated directly from Alzheimer's brains impair synaptic plasticity and memory. *Nat. Med. 14*, 837–42

30. Venegas, C., Kumar, S., Franklin, B. S., Dierkes, T., Brinkschulte, R., Tejera, D., Vieira-Saecker, A., Schwartz, S., Santarelli, F., Kummer, M. P., Griep, A., Gelpi, E., Beilharz, M., Riedel, D., Golenbock, D. T., Geyer, M., Walter, J., Latz, E., and Heneka, M. T. (2017) Microglia-derived ASC specks cross- seed amyloid-β in Alzheimer's disease Genetic and experimental evidence supports a pathogenic role of immune activation in neurodegenerative disorders. *Nature. 552*, 355-361.

31. Li, L., Li, C., Zhang, Z., and Alexov, E. (2013) On the dielectric "constant" of proteins: Smooth dielectric function for macromolecular modeling and its implementation in DelPhi. *J. Chem. Theory Comput. 9*, 2126–2136

32. Chattopadhyay, A., and Mukherjee, S. (1999) Red Edge Excitation Shift of a Deeply Embedded Membrane Probe: Implications in Water Penetration in the Bilayer. *J. Phys. Chem. B. 103*, 8180-8185.

33. Mcdowall, J. S., Ntai, I., Hake, J., Whitley, P. R., Mason, J. M., Pudney, C. R., and Brown, D. R. (2017) Steady-State Kinetics of α-Synuclein Ferrireductase Activity Identifies the Catalytically Competent Species. *Biochemistry. 56,* 2497-2505

34. Fields G. B. & Noble, R. L. (1999) Solid-phase peptide synthesis utilizing 9-fluorenylmethoxycarbonyl amino acids. *Int. J. Pept. Protein Res. 35*, 161–214

35. Zagorski, M. G., Yang, J., Shao, H., Ma, K., Zeng, H. & Hong, A. (1999) Methodological and chemical factors affecting amyloid β-peptide amyloidogenicity. *Methods Enzymol 309*, 189-203.

Supplementary information - An excitation-energy-dependent molecular beacon detects early-stage neurotoxic Aβ aggregates in the presence of cortical neurons.

Christina E. Gulácsy[1], Richard Meade[1], Dragana A.M. Catici[1], Christian Soeller[4], G.Dan Panto[§3], D. Dafydd Jones[5], Dominic Alibhai[6], Mark Jepson[6], Ventsislav K. Valev[2], Jody M. Mason[1]*, Robert J. Williams[1]*, Christopher R. Pudney[1]*

[1]Department of Biology and Biochemistry, [2]Department of Physics, [3]Department of Chemistry, University of Bath, Bath, United Kingdom.[4]Biomedical Physics, University of Exeter, Exeter, United Kingdom.[5]School of Biosciences, Cardiff University, Cardiff, United Kingdom. [6]Wolfson Bioimaging Facility, University of Bristol, Bristol United Kingdom.

Supplementary figures

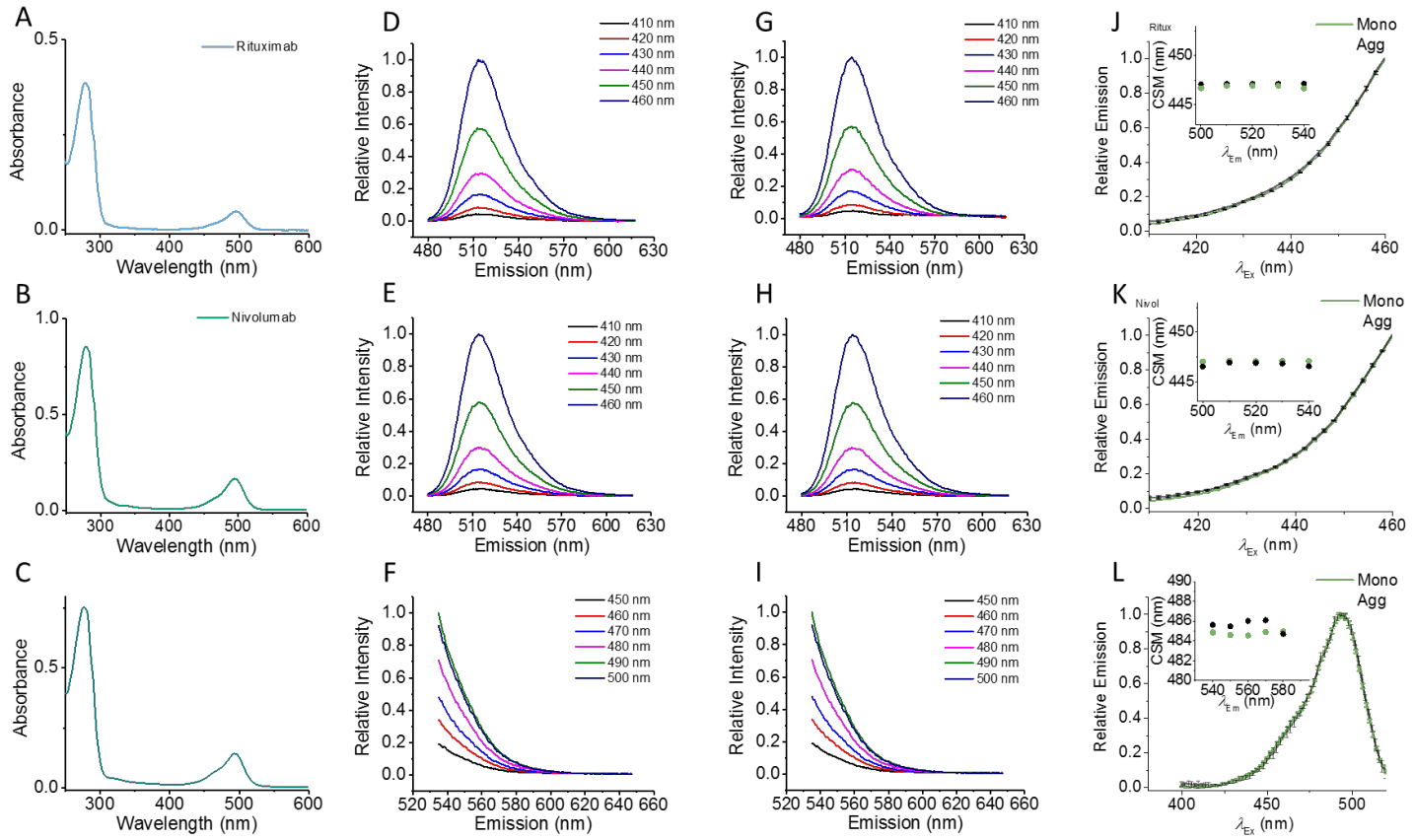

Figure S1. Absorption, emission and excitation spectra of fluorophore labelled antibodies both monomeric and aggregated. Top row show Rituximab-Alexa 488 data, middle row shows Nivolumab-Alexa 488 data and the bottom row shows Rituximab-Fluorescein data. **A-C,** Absorption spectra of Alexa 488 labelled Rituximab (**A**), Nivolumab (**B**) and fluorescein labelled Rituximab (**C**). The ratio of extinction coefficients for the protein (280 nm) and the dye (~500 nm) suggests approximately 0.5 molar equivalents of fluorophore are bound to the antibodies in all cases. **D-F,** Sample EEM spectra for monomeric (assessed by DLS) mAbs. **G-I,** Sample EEM spectra for aggregated (assessed by DLS) mAbs. Note that the Stokes shift of the fluorophore determines how much of the emission spectrum can be present and not be convolved of the excitation light, with this being the reason for the difference in the spectra between Alexa 488 and fluorescein. **J-L,** Comparison of excitation spectra for both monomeric (green line) and aggregated (black line) mAbs. The excitation spectra shown are the average normalized values across the range of emission wavelengths and the error bars on each data point represent the standard deviation of the normalized spectra. That is, the very small error bars illustrate that the excitation spectrum at each emission wavelength essentially overlay and that the excitation spectra for both the monomeric and aggregated proteins overlay. *Inset* is the CSM of the excitation spectra at a range of different emission wavelengths, where CSM is calculated in the same way as described in the main text. The CSM values are essentially invariant at each emission wavelength and this is quantifiable evidence that the excitation spectra are identical. Variation in excitation spectra is, therefore, not the cause of the observed fluorescence edge-shift.

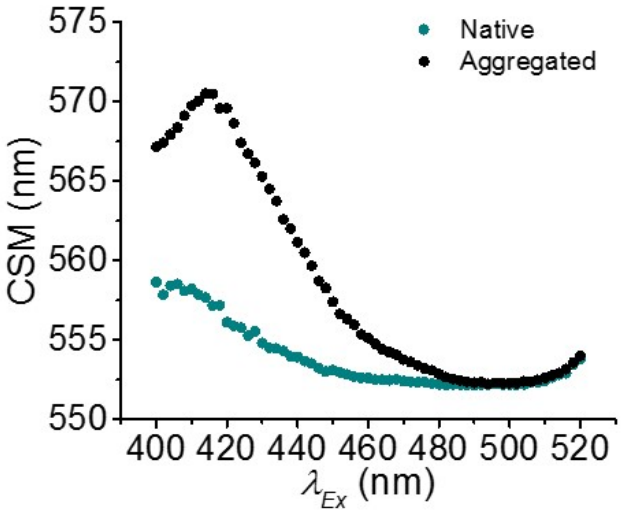

Figure S2. Fluorescein labeled Rituximab shows an excitation-energy-dependent blue-shift when aggregated, similar to the Alexa 488 labelled mAbs.

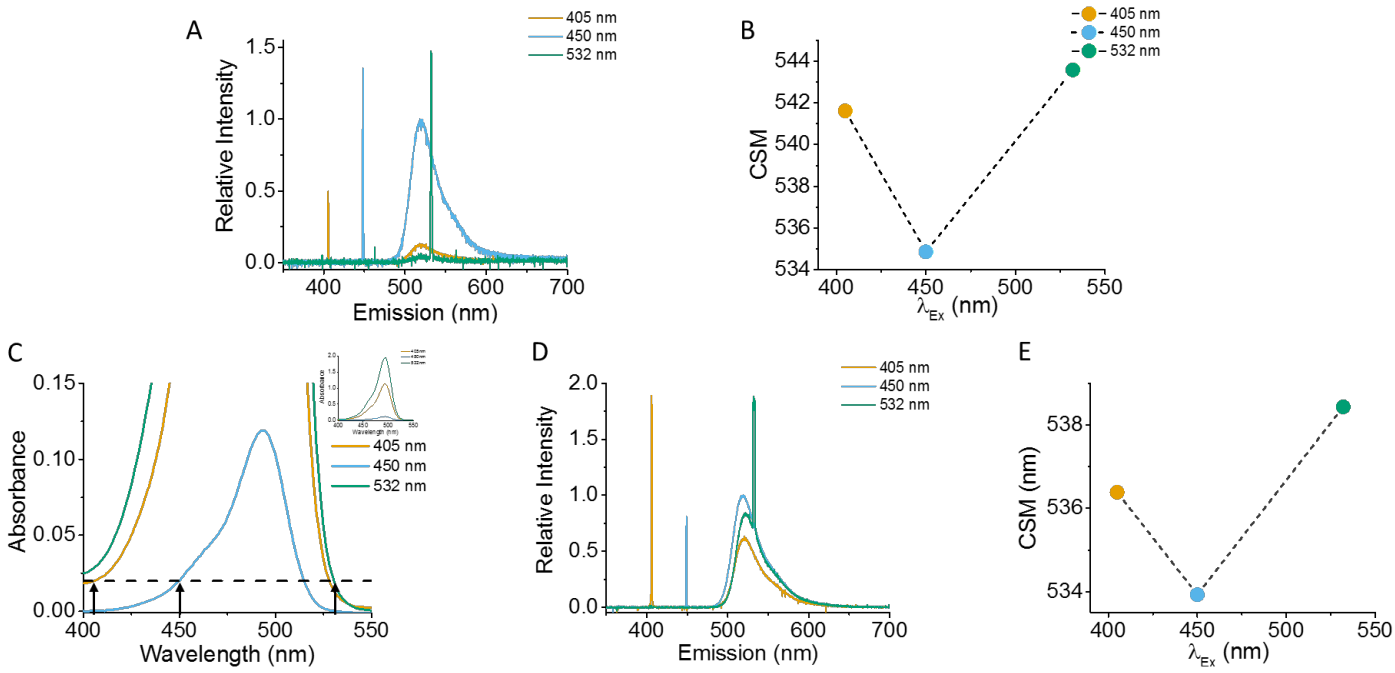

Figure S3. A, Raw emission spectra obtained for λ_{Ex} 405, 450, and 532 nm by 4.9 mW lasers. **B,** Extracted CSM from emission spectra in **A**. CSM values were calculated from emission data fitted with skewed Gaussians following subtraction of laser lines. Following observation of the blue-shift in the laser study, an additional experiment was carried out to determine if the blue-shift was due to the laser intensity. Three solutions of Alexa 488 in water were made in order to match the absorptions at the specified laser wavelengths, as shown by **C**, with arrows indicating matching absorbance at 405, 450, and 532 nm. Subsequent laser emission studies of Alexa 488 from **C** are shown in Panel **D**. **E,** Extracted CSM from emission spectra in **D.** CSM values were calculated from emission spectra from 450 to 650 nm following removal of the 532 nm laser line (530 to 535 nm) of all spectra. The blue-shift was still observed, demonstrating it is not artefactual and the excitation of the fluorophore is unaffected across the emission range studied.

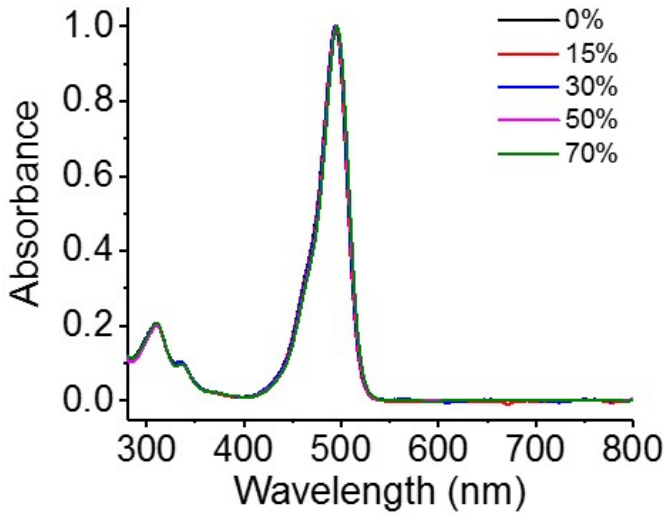

Figure S4. Normalized absorption spectra (normalized for concentration differences only) for Alexa-488 in different percentages of methanol (see key).

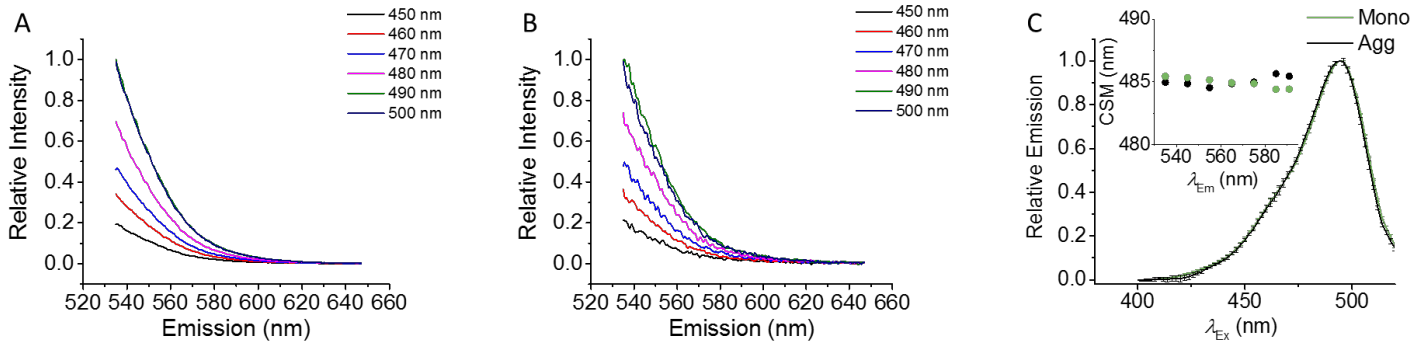

Figure S5. A, Sample EEM spectra for monomeric $A\beta_{15-21}$-fluor. **B,** Sample EEM spectra for aggregated $A\beta_{15-21}$-fluor (aggregation assessed by DLS as in main manuscript). **C,** Comparison of excitation spectra for both monomeric (green line) and aggregated (black line) protein. The excitation spectra shown are the average normalized values across the range of emission wavelengths and the error bars on each data point represent the standard deviation of the normalized spectra. That is, the very small error bars illustrate that the excitation spectrum at each emission wavelength essentially overlay and that the excitation spectra for both the monomeric and aggregated proteins overlay. *Inset* is the CSM of the excitation spectra at a range of different emission wavelengths, where CSM is calculated in the same way as described in the main text. The CSM values are essentially invariant at each emission wavelength and this is quantifiable evidence that the excitation spectra are identical. Variation in excitation spectrum is therefore not the cause of the observed fluorescence edge-shift.

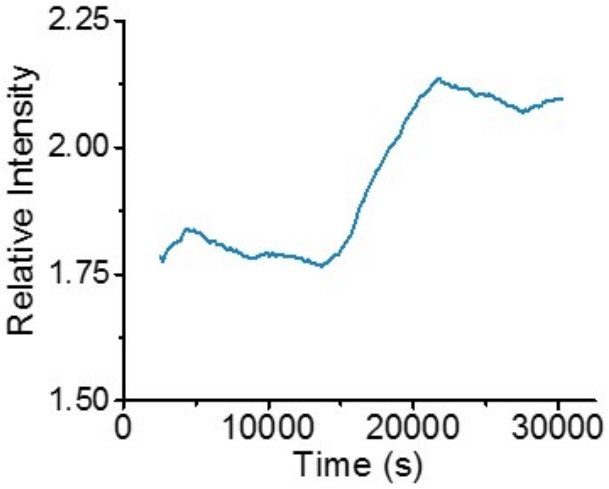

Figure S6. ThT assay of 100 μM A$\beta_{15\text{-}21}$-fluor fluorescein labelled A$\beta_{15\text{-}21}$. The increase in emission is indicative of the formation of fibrillar aggregates. We note that the absolute emission change is relatively small since we anticipate there is a very large amount of resonance energy transfer between the fluorescein and the ThT. This will not affect the aggregation kinetics but will lead to an apparent quenching of the ThT emission. *Conditions,* 90 μM ThT in 50 mM phosphate buffer pH 7, λ_{Em} 482 nm at λ_{Ex} 450 nm.

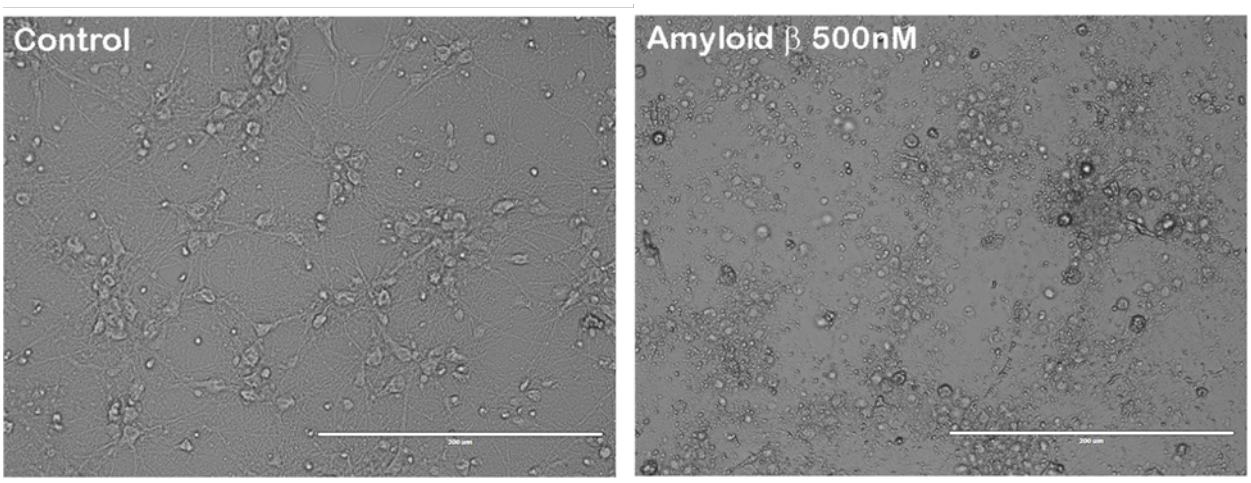

Figure S7. Primary mouse cortical neurons treated for 24 hours with $A\beta_{15\text{-}21}$-fluor (500 nM), washed with PBS, then fixed in paraformaldehyde (4 %). Right images show neurotoxicity compared to control.

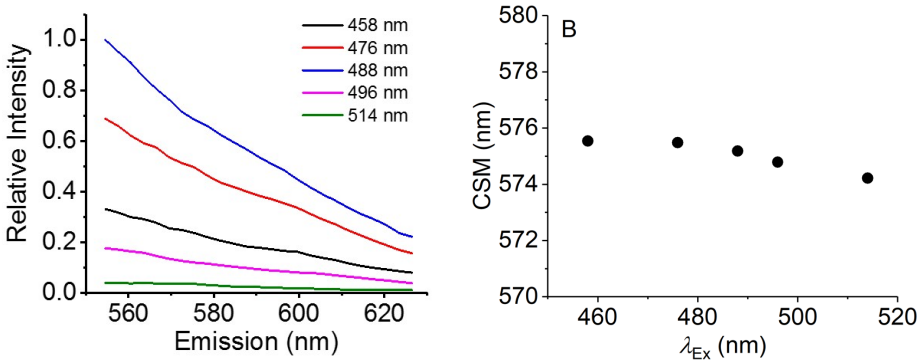

Figure S8. (A) Raw EEM data for fluorescein imaged on the same microscopy platform as the whole cell images in Figure 2. **(B)** The corresponding CSM *versus* λ_{Ex} plot.

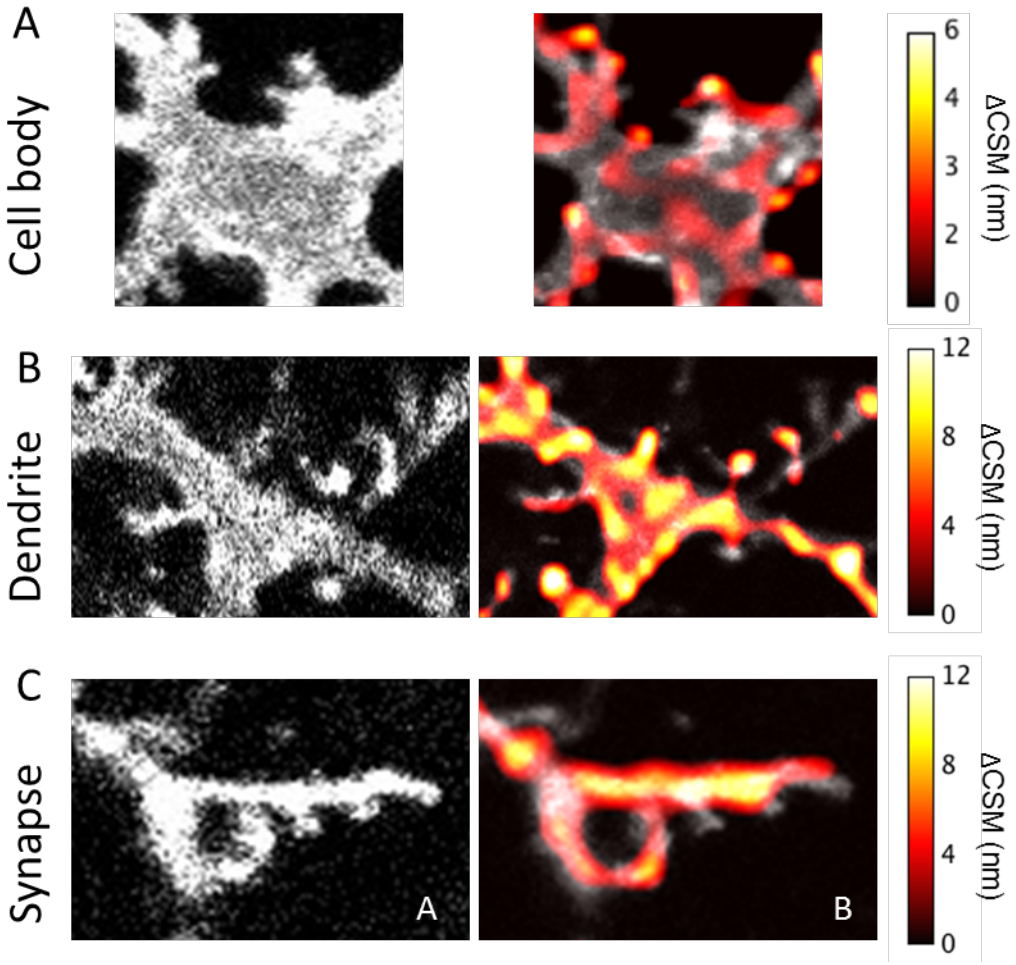

Figure S9. Enlarged image of **A,** the cell body in Figure 2A, **B,** the dendrite in Figure 2B and **C,** the putative synapse in Figure 2B. The left-hand panel in each case shows $A\beta_{15\text{-}21}$-fluor emission and the right hand panel shows the extracted edge-shift values.

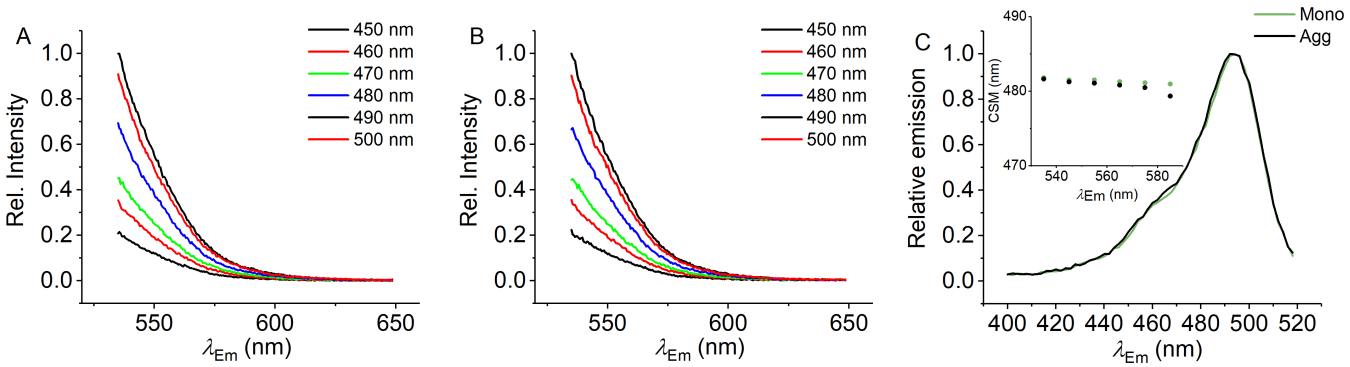

Figure S10. A, Sample EEM spectra for monomeric $A\beta_{1\text{-}40}$-fluor (assessed by DLS). **B,** Sample EEM spectra for aggregated $A\beta_{1\text{-}40}$-fluor (assessed by DLS). **C,** Comparison of excitation spectra for both monomeric (green line) and aggregated (black line) protein. The excitation spectra shown are the average normalized values across the range of emission wavelengths. *Inset* is the CSM of the excitation spectra at a range of different emission wavelengths, where CSM is calculated in the same way as described in the main text.

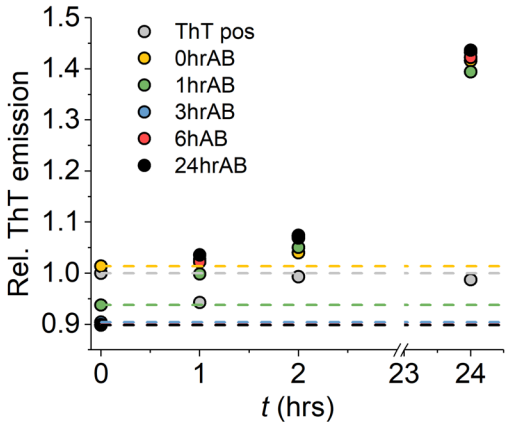

Figure S11. Change in ThT emission as a function of time for flour$A\beta_{1\text{-}40}$ aged for different times, prior to monitoring ThT emission. We note the change in emission is relative to the background ThT emission and so represents an essentially negligible change in all cases.

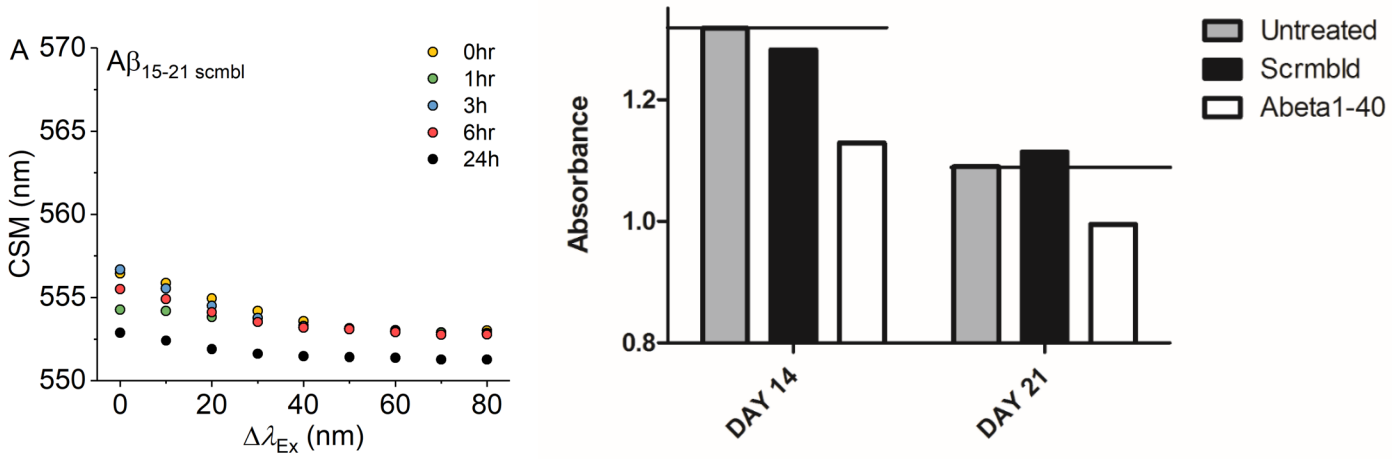

Figure S12. A) Edge-shift measurements for the scrambled flour-$A\beta_{15\text{-}21}$ aged for different time periods. Essentially no meaningful change in ΔCSM is observed. **B)** MTT absorbance (595 nm) for cells in the presence of 500nm of each peptide (incubated overnight).

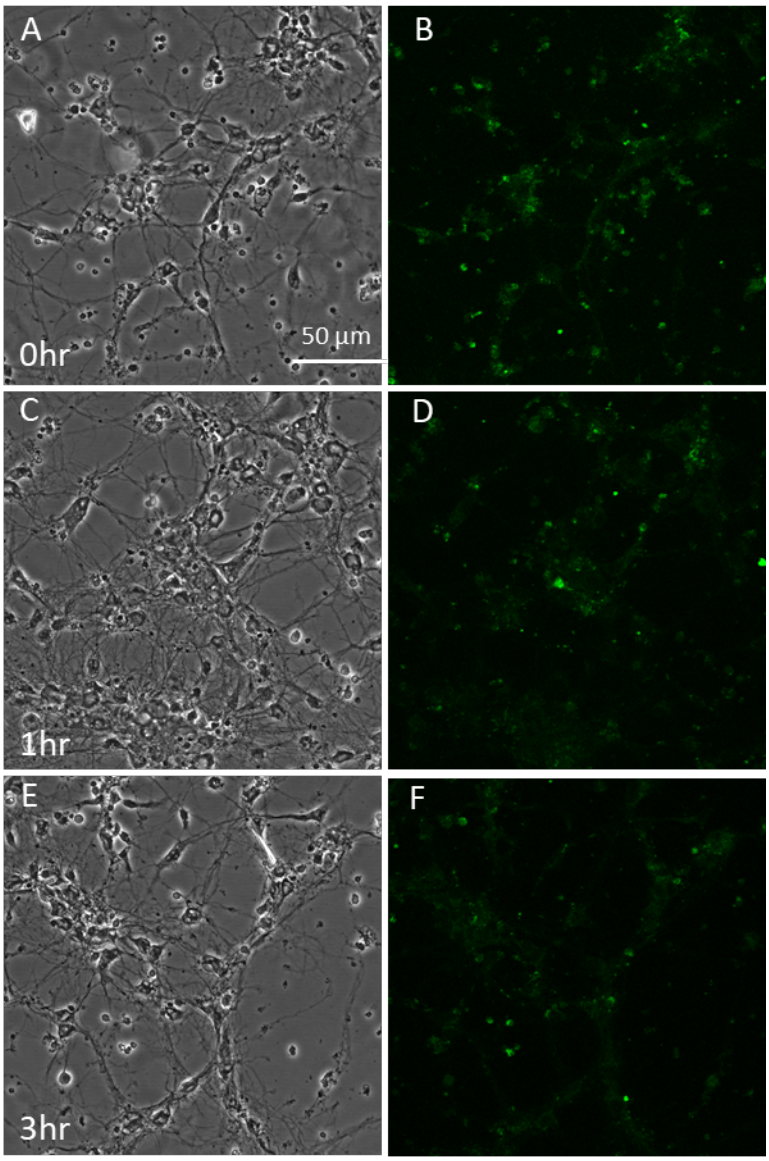

Figure S13. Mouse cortical neurons treated with aged 500 nM fluor-A$\beta_{1\text{-}40}$ at 0 hr (A), 1 hr (C) and 3 hrs (E). The panels at right of each condition show a corresponding fluorescence emission image ($\lambda_{Ex458nm}$; panels B, D and F). Image settings are the same for both Figures S13 and Figures 6.

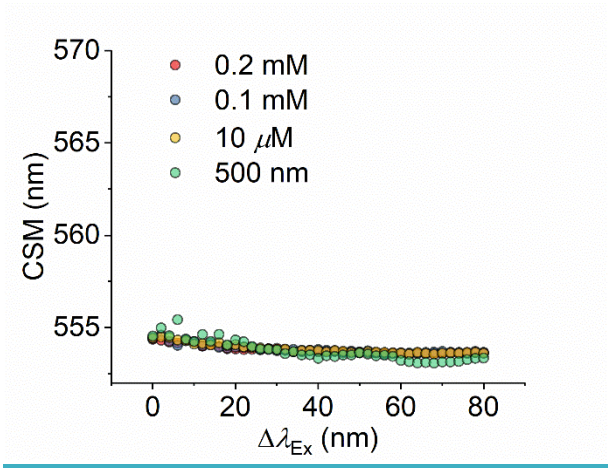

Figure S14. Edge-shift for a range of Aβ1-40 concentrations. Scale bars are the same as Figure 5 for comparison.

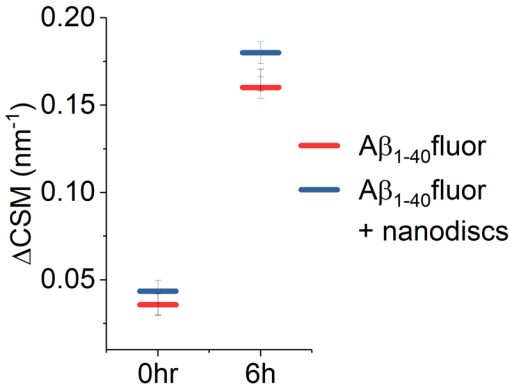

Figure S15. Edge-shift for $A\beta_{1\text{-}40}$ in the presence and absence of nanodiscs and aged for 6 hours at 25 °C.